THE ASTROPHYSICAL JOURNAL, 289:634–643, 1985 February 15

STELLAR WINDS DRIVEN BY SUPER-EDDINGTON LUMINOSITIES

THOMAS QUINN AND BOHDAN PACZYŃSKI[1,2]
Princeton University Observatory
Received 1984 April 16; accepted 1984 August 29

ABSTRACT

We constructed over 100 models of a steady-state, spherically symmetric outflow of gas from a star of 1.4 $M_\odot$ with a pure helium envelope and a luminosity somewhat exceeding the Eddington limit. We used Newtonian gravity and a nonrelativistic equation of motion but crudely allowed for the sphericity of the atmospheres of our models. Super-Eddington luminosities were made possible by the decrease of the electron-scattering opacity at the high temperature at which accreted helium burns on neutron stars.

We explored a large region in the mass-loss rate ($\dot{M}$)–energy-loss rate ($\dot{E}$) diagram, and we found self-consistent models for $1.01 < \dot{E}/L_{\rm Edd} < 1.11$, and for $16.5 < \log \dot{M} < 19.5$ (in grams per second). Outflow velocities at infinity never exceeded 3% of the speed of light, and were usually much smaller. The kinetic energy flux never exceeded $10^{-3} L_{\rm Edd}$.

Our models have photospheric radii much larger than neutron star radii, and they are faint in the X-ray region of the spectrum. These models may be relevant to some very strong and long X-ray bursts with precursors, with no X-ray emission detected between the precursor and the main burst. It is during that phase that the slightly super-Eddington luminosity may be responsible for a large radius expansion and a steady-state, radiation-driven wind.

Subject headings: stars: interiors — stars: neutron — stars: winds — X-rays: bursts

I. INTRODUCTION

Mass loss from stars is a well-observed phenomenon, and various models have been proposed to explain it. Models of stationary spherically symmetric mass outflow are very popular. In a steady-state model the flow is subsonic at small radii and supersonic at infinity, passing through a critical point where the outflow velocity is equal to the speed of sound. Radiation pressure in lines may be the driving force for mass outflow from hot stars, while radiation pressure on dust grains may be important for cool supergiants (see Cassinelli 1979 for a review). In both cases, a large opacity above the critical point is responsible for the mass outflow. This large opacity occurs above the photosphere, and the critical point is at a small optical depth. These optically thin winds are powered by *momentum* transfer from radiation to gas, and the mass-loss rate $\dot{M}$ is limited:

$$\dot{M} < \frac{L}{vc}, \tag{1}$$

where L is the luminosity, v is the outflow velocity, and c is the speed of light. Much higher mass-loss rates are possible when the critical point is at a large optical depth. In that case *energy* may be transferred from radiation to the gas flow, and the limit (1) may be multiplied by the optical depth at the critical point. Such conditions may be present in some novae and symbiotic stars (Meier 1982*c*, and references therein) and in some X-ray bursters (Kato 1983; Ebisuzaki, Hanawa, and Sugimoto 1983).

In this paper we study mass outflow driven by radiation pressure, with a critical point located at large optical depth. Our models also require a larger continuum opacity above the critical point than in the deep stellar interior. Early attempts to build similar models relied on a huge opacity maximum in the zones of partial hydrogen and helium ionization (Żytkow 1972, and references therein). Unfortunately, when the density is low, the opacity peak due to ionization almost vanishes, and radiation cannot be used efficiently to drive the mass outflow. Żytkow (1972, 1973) found that no models of this type were self-consistent because they had more mass above the critical point than below it. A steady-state outflow requires the opposite to be true.

If the luminosity is super-Eddington, then electron scattering is the only opacity needed to drive the mass outflow. However, if Thomson scattering is used throughout the model, then ordinary stars cannot generate a radiation-driven wind. This is because the radiative flux from the deep interior is limited by the same value of the opacity as that used in the outermost zones, and it is not possible to obtain a super-Eddington radiative luminosity. On the other hand, nonstandard models with mass and energy injected with a freely chosen rate at some radius below a critical point can generate such winds (Meier 1982*a*, *b*, *c*, and references therein).

Recently, more conventional stellar models have been found to provide super-Eddington luminosity. These are models of strong X-ray bursts due to helium shell flashes on accreting neutron stars (Hanawa and Sugimoto 1982; Taam 1982; Wallace, Woosley, and Weaver 1982; Paczyński 1983). During the flash the maximum temperature in the nuclear burning region exceeds 10^9 K, and the electron-scattering opacity is reduced because of relativistic electron velocities. The corresponding Compton scattering opacity is well below the Thomson value (see Buchler and Yueh 1976 for opacity tables), and radiation may diffuse from the nuclear-burning region at a super-Eddington rate. This radiation flux pushes out the relatively cool surface layers, where the opacity cannot drop below the Thomson limit even if the density becomes very small. There is a distinct possibility here of establishing a steady-state stellar wind driven by super-Eddington luminosity with no ad

[1] On leave from N. Copernicus Astronomical Center, Polish Academy of Sciences.
[2] A long-term member, Institute for Advanced Study, Princeton.

hoc injection of mass or energy somewhere below the critical point. In fact, a few such models were recently published by Ebisuzaki, Hanawa, and Sugimoto (1983) and by Kato (1983), and were also reported by Melia and Joss (1983). These models may be relevant to very long X-ray bursts with precursors, where observations indicate very large expansions of the photospheric radii of bursting neutron stars (Tawara *et al.* 1984; Lewin, Vacca, and Basinska 1984).

The aim of this paper is to establish a region in the $\dot{M}-\dot{E}$ plane (i.e., in the mass-loss rate–energy-flow rate plane) where models of steady-state stellar winds driven by the radiation pressure on free electrons are possible. We improve the treatment of the outer boundary condition, but we use Newtonian gravity, just as previous investigators have done. There are two reasons for this. We wanted to make our survey of the $\dot{M}-\dot{E}$ plane as simple as possible, and we also wanted to keep our assumptions close to those of other studies, to simplify the comparison. There are many improvements to be made in our models before meaningful comparisons can be made, not only with other models but also with observations. However, we found the present model situation so confusing that we decided to clarify it somewhat before investing much more effort and time in truly state-of-the-art computations. We find a full range of simple but reasonable models, and we find a range of parameters, $\dot{M}$ and $\dot{E}$, for which various physical effects should be treated more carefully.

II. COMPUTATIONAL METHOD AND INPUT PHYSICS

Throughout this paper we adopted Newtonian equations of motion as well as Newtonian gravity. For the equation of state we used a mixture of perfect, fully ionized, and nondegenerate gas with radiation. For simplicity we considered pure helium only. The only nuclear reaction was 3α with the rate given by Fowler, Caughlan, and Zimmerman (1975). The only opacity was from electron scattering. It was calculated with a formula

$$\kappa_e = 0.2\left[1+\left(\frac{T}{4.5\times 10^8\ \mathrm{K}}\right)^{0.86}\right]^{-1} \tag{2}$$

(see Paczyński 1983), which approximates the tables of Buchler and Yueh (1976) with a 2% accuracy in the nondegenerate limit. All our models were dominated by radiation pressure. Electron degeneracy was negligible, and opacities other than electron scattering were very small.

Models of radiatively driven winds with a critical point at a large optical depth have very diffuse photospheres with the density scale height approximately equal to the local radius. Therefore, the variation of radiation energy density with radius is due not only to diffusion through opaque matter, but also to geometrical dilution. Let us define an optical depth-like parameter τ^*:

$$\tau^* = \kappa\rho r\ , \tag{3}$$

where κ is the opacity, ρ is the density, and r is the radius. At large optical depth the diffusion approximation is good, and we may calculate the radiation energy density, U_r, and its gradient as

$$U_r = aT^4\ ,\quad \frac{dU_r}{dr} = -\frac{3\kappa\rho F_r}{c}\ ,\quad \tau^* \gg 1\ (\mathrm{LTE})\ , \tag{4}$$

where F_r is the radiative energy flux, defined as

$$F_r = \frac{L_r}{4\pi r^2}\ , \tag{5}$$

L_r is the luminosity at radius r, and all other symbols have their usual meaning. When the optical depth is small, the radius is large, and geometrical dilution is dominant, we may write

$$U_r = \frac{F_r}{c}\ ,\quad \frac{dU_r}{dr} = \frac{L_r}{2\pi r^3 c}\ ,\quad \tau^* \ll 1\ (\text{streaming radiation})\ . \tag{6}$$

In general, we may need a gradual transition between equations (4) and (6), and there is no simple and exact description of the radiation energy density and its gradient in this case. Following Paczyński (1969), we approximate the gradient with a sum of the two limiting cases (4) and (6) to obtain

$$\frac{dU_r}{dr} = -\frac{3\kappa\rho L_r}{4\pi r^2 c} - \frac{L_r}{2\pi r^3 c} = -\frac{3\kappa\rho L_r}{4\pi r^2 c}\left(1+\frac{2}{3\kappa\rho r}\right). \tag{7}$$

This new simple approximate equation has the correct asymptotic limits for $\tau^* \gg 1$ and for $\tau^* \ll 1$, but its accuracy in the transition region should be questioned.

Mihalas (1978, p. 246, eq. [7-181]) gives a simple expression for the variation of the radiation energy density with radius in extended atmospheres where τ^* varies as a power of radius. According to Mihalas,

$$U_r = \frac{L_r}{4\pi r^2 c}\left(1+3\tau\,\frac{n-1}{n+1}\right). \tag{8}$$

According to Hummer and Rybicki (1971), differences between this analytical formula and their accurate numerical solutions are on the order of 5%–10% when

$$\tau^* \equiv \kappa\rho r = \alpha r^{-(n-1)}\ ,\quad n>1\ ,\quad \alpha = \mathrm{const.} \tag{9}$$

The optical depth τ may be calculated as

$$\tau = \int_r^\infty \kappa\rho dr' = \frac{\alpha r^{-(n-1)}}{n-1} = \frac{\tau^*}{n-1}\ . \tag{10}$$

Differentiating U_r, given by equation (8), with respect to r, we obtain our equation (7). Therefore, equation (7) should be reasonably accurate even in the transition region, where $\tau^* \approx 1$, provided the relation (9) is satisfied. Of course, we do not know *a priori* how τ^* will vary with radius in a model of a stellar wind. Therefore, rather than equation (8), we use the differential equation (7), since this can be integrated without knowing the global solution. It turns out that variations of τ^* with radius may be roughly approximated with a power law in our solutions (see Fig. 4 for the variation of $\kappa\rho r$ with r), and so it is reasonable to use the equation (7) to calculate variations of radiation energy density.

When electron scattering dominates, the radiation may be far from LTE even at moderately large optical depths, and it may be difficult to assign it any temperature. This is not very important for our models because the temperature, as opposed to the radiation energy density, is only needed to calculate the opacity and gas pressure. At temperatures below 10^8 K gas pressure is not very important in our models, while the opacity is almost exactly equal to the Thomson value and does not depend on temperature. By the time the temperature reaches 10^8 K the optical depth is so large that LTE holds with high accuracy. Therefore, we use the temperature throughout our models as a variable directly related to the radiation energy density: $aT^4 = U_r$. It should be remembered, however, that this temperature is just a convenient parameter to be used in our equations at low and moderate optical depths, and it has

its full physical significance only at large optical depths. Of course, the spectrum of radiation emerging from the photosphere may be considerably different from the Planck spectrum corresponding to any temperature (see London, Howard, and Taam 1984).

Except for our treatment of temperature gradient at low optical depths we adopted the equations for a steady-state radiation driven wind in an almost identical form as that used by Żytkow (1972), Cassinelli and Castor (1973), and Kato (1983). Our fundamental equations are those of mass conservation, energy conservation, equation of motion, and the one for temperature gradient:

$$4\pi r^2 \rho v = \dot{M} = \text{const} . \tag{11a}$$

$$\dot{M}\left(\frac{v^2}{2} - \frac{GM}{r} + \frac{U+P}{\rho}\right) + L_r = \dot{E} = \text{const} . \tag{11b}$$

$$v\frac{dv}{dr} + \frac{GM}{r^2} + \frac{1}{\rho}\frac{dP_g}{dr} - \frac{\kappa L_r}{4\pi r^2 c} = 0 . \tag{11c}$$

$$\frac{dT}{dr} = -\frac{3\kappa\rho L_r}{16\pi r^2 c a T^3}\left(1 + \frac{2}{3\kappa\rho r}\right) . \tag{11d}$$

These are supplemented with additional algebraic relations for the equation of state and the opacity,

$$P_g = \frac{k}{\mu H}\rho T , \quad P_r = \frac{a}{3}T^4 , \quad U = 1.5P_g + 3P_r , \tag{12}$$

where all the symbols have their usual meaning, $\mu = 4/3$ for pure fully ionized helium, and the opacity κ is given with equation (2). Notice that in all these equations we define L_r as the radiative luminosity in a frame *comoving* with the flow. The luminosity as seen by a stationary observer would be $(1 + 2v/c)$ times larger (see Cassinelli and Castor 1973 for a detailed discussion).

To start our outflow integrations from the outside we adopted the following procedure. First, we chose the global parameters, which defined the model: the total mass M, the mass-loss rate $\dot{M}$, and the total energy outflow rate $\dot{E}$. We guessed an outflow velocity at infinity, v_∞. We could then calculate the radiative luminosity as seen by a stationary observer at infinity:

$$L_\infty = \dot{E} - \dot{M}\frac{v_\infty^2}{2} . \tag{13a}$$

Then we calculated the radiative luminosity at large radii in the frame *comoving* with the wind according to a formula provided by Cassinelli and Castor (1973):

$$L_r = L_\infty \Big/ \left(1 + 2\frac{v_\infty}{c}\right) . \tag{13b}$$

In the region which is optically very thin L_r may be assumed to be constant, and if the gas pressure is ignored, then equation (11c) may be integrated to obtain

$$v^2 = v_\infty^2 + \frac{2GM}{r} - \frac{\kappa L_r}{2\pi r c} . \tag{13c}$$

The density and "temperature" of the flow were calculated then as

$$\rho = \frac{\dot{M}}{4\pi r^2 v} , \quad T = \left(\frac{L_r}{4\pi r^2 c a}\right)^{0.25} . \tag{13d}$$

Since all the variables L_r, v, ρ, T had been defined, it was then possible to integrate the equations (11) inward, through the photosphere, toward the critical point.

There are some additional limitations of our treatment. At very small optical depths and negligible gas pressure we still used our equation (6) to calculate the radiation energy density, and we adopted our equation (12) for the radiation pressure. In this approximation equation (11b) may be written as

$$\dot{E} = \dot{M}\left(\frac{v^2}{2} - \frac{GM}{r} + \frac{4U_r}{3\rho}\right) + L_r$$
$$= \dot{M}\left(\frac{v^2}{2} - \frac{GM}{r}\right) + L_r\left(1 + \frac{4v}{3c}\right) . \tag{14}$$

The last term in that equation, $4v/3c$, is not correct. According to Cassinelli and Castor (1973) it should be $2v/c$. This term should allow for the difference between the luminosity as seen by an oberver comoving with the flow and the luminosity as seen by a stationary observer, because of a first-order Doppler effect. We use a correct formula (eq. [13b]) to start our integrations, but our integral equation (11b) has a somewhat incorrect formulation at very small optical depth. This is not a large error, since all our models had $v/c \ll 1$. However, it is one reason why our simplified equations cannot be used for models with a critical point located at small or moderate optical depth.

Given the starting condition at a large, but finite radius, we can use the four basic equations (11a)–(11d), two differential and two algebraic, to integrate a model inward. We found it convenient to replace equation (11c) with the equivalent equation for density gradient:

$$\frac{d\rho}{dr} = \left[\frac{2\rho v^2}{r} - \frac{GM\rho}{r^2} - \left(\frac{\partial P_g}{\partial T}\right)_\rho \frac{dT}{dr} + \frac{\kappa\rho L_r}{4\pi r^2 c}\right]\left[\left(\frac{\partial P_g}{\partial \rho}\right)_T - v^2\right]^{-1} , \tag{15}$$

which was obtained combining equations (11a) and (11c). It shows explicitly the presence of a critical, i.e., sonic point, where the velocity of outflow is equal to the isothermal sound speed, and the denominator and numerator of equation (15) must vanish simultaneously. So, we finally used two differential equations, (11d) and (15), and two algebraic equations, (11a) and (11b). The radius was the independent variable, and density, temperature, velocity, and luminosity were the four fundamental variables to be found. We used auxiliary algebraic equations (12) and (2) to evaluate pressure, internal energy, and opacity. The integrations were carried inward until a divergence of numerical solutions indicated that we were approaching a critical (sonic) point.

We also started integrations from the critical point in a standard way, as described by Żytkow (1972) and Kato (1983), for example. For a given stellar mass, mass-loss rate, and energy-loss rate we needed one additional parameter, which we chose to be the critical radius, r_c. We integrated outward and tried to match the solution with that carried inward from infinity. We had two ordinary differential equations, (11c) and (11d), and two adjustable parameters, r_c and v_∞. This fitting procedure allowed us always to find just one set of adjustable parameters; i.e., we could obtain a unique solution for the given values of M, $\dot{M}$, and $\dot{E}$. Once the location of the critical point had been established by this fitting procedure, we integrated our equations (11a)–(11d) from the critical point inward. This time we also integrated the nuclear luminosity from helium burning

through the 3α reaction. The integrations were stopped when one of the following conditions had been satisfied:

1. The radiative luminosity dropped to zero as a result of helium burning.
2. The radius decreased to the gravitational radius defined as $r_g \equiv 2GM/c^2$.
3. The temperature increased above 5×10^9 K.

The main possible application of our models is to neutron stars undergoing strong nuclear flashes in the accreted matter. It is likely that super-Eddington luminosities are reached in such objects when almost all the nuclear fuel has been burned. Therefore, our choice of pure helium matter and our calculations of the helium-burning rate may seem to be not very relevant. However, we treat our nuclear-burning calculation only as a rough indication that our solutions are already deep into the interior of our model. Also, we expect that the results would be qualitatively the same for any other choice of chemical composition, provided the models were chemically homogeneous throughout the outflowing steady-state region. In fact, chemical homogeneity is a necessary condition for the validity of a steady-state approximation. The other important condition is that there should be more mass below the critical point (but above the base of the accreted layer as approximated by the nuclear burning shell) than between the critical point and the photosphere. Of course, in a strictly steady-state model of the outflow the amount of matter above the photosphere is logarithmically infinite. However, the flow above the photosphere is highly supersonic and optically thin; therefore, it does not have much dynamical or thermal effect on the flow below the photosphere. For this reason we ignored matter above the photosphere for the mass balance used to verify the applicability of the steady-state assumption. Notice that while obtaining our models we were solving a two-point boundary value problem. One boundary condition (dynamical) had to be satisfied at the critical point. The second boundary condition (thermal) had to be satisfied at the photosphhere, or at any small optical depth (see eq. [13d]).

III. RESULTS

All models were computed for a star with a mass $M = 1.4\ M_\odot$, with a pure helium outflowing envelope. For such a star the Eddington luminosity is defined as

$$L_{\rm Edd} = \frac{4\pi cGM}{0.2(1+X)} = 2.50 \times 10^{38}\ {\rm ergs\ s^{-1}} \times \frac{M}{M_\odot} = 65300\ L_\odot \times \frac{M}{M_\odot}. \quad (16)$$

We parametrized our models with two integration constants: the mass-loss rate $\dot{M}$ measured in grams per second, and the total energy-loss rate $\dot{E}$ measured in units of the Eddington luminosity $L_{\rm Edd}$.

We calculated a total of 140 models using the technique described in the previous section. They are shown in the $\dot{M}-\dot{E}$ plane in Figure 1. The models we consider acceptable are indicated with filled circles, and they cover the area within the border drawn with a dashed line. Various segments of that line will be described below. The three models calculated by Kato (1983) are shown with large open circles. The analytical models of Meier (1982*a*, *b*, *c*) correspond to our solutions with adiabatic interiors and are in the large region with the borders schematically shown with a dotted line. The lower dotted line is where our models become adiabatic, and the upper dotted line is where the critical point becomes close to the gravitational radius. Meier's models are outside our region of acceptability because they all have more mass between the photosphere and the critical point than between the critical

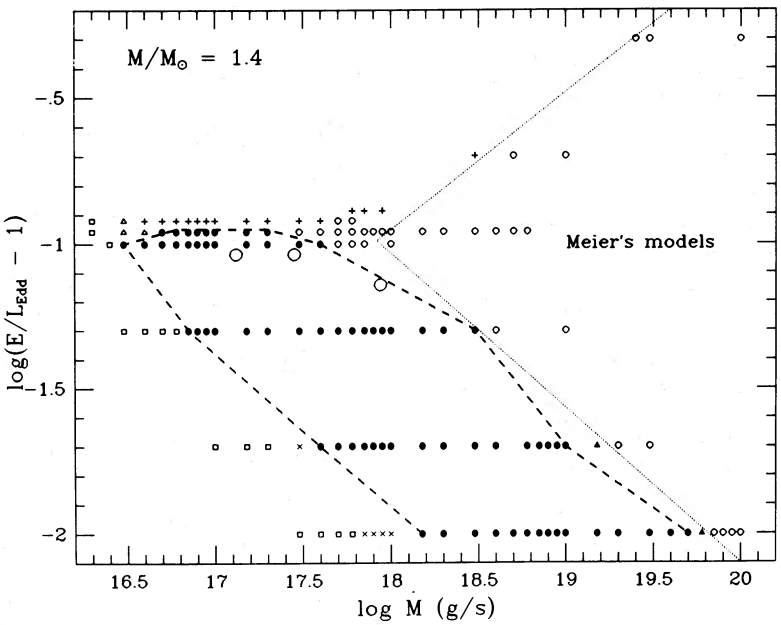

FIG. 1.—Position of our models on the $\dot{M}-\dot{E}$ plane. The acceptable models are indicated by the filled circles and are enclosed by the dashed line. Various segments of that line are explained in Figs 2*a*, 2*b*, and 2*c*. The models for which Meier's approximations are good are to the right of the dotted line. The squares are models with optically thin critical points. The crosses are models with $\kappa\rho r$ at the critical point less than 10. The open triangles are points with the critical radius below the gravitational radius. The plusses are points with the critical radius less than 1.2 times the gravitational radius. The open circles are points with adiabatic solutions. The filled triangle is a point with the mass criterion for the steady-state approximation not satisfied. The large open circles with dots represent the models of Kato.

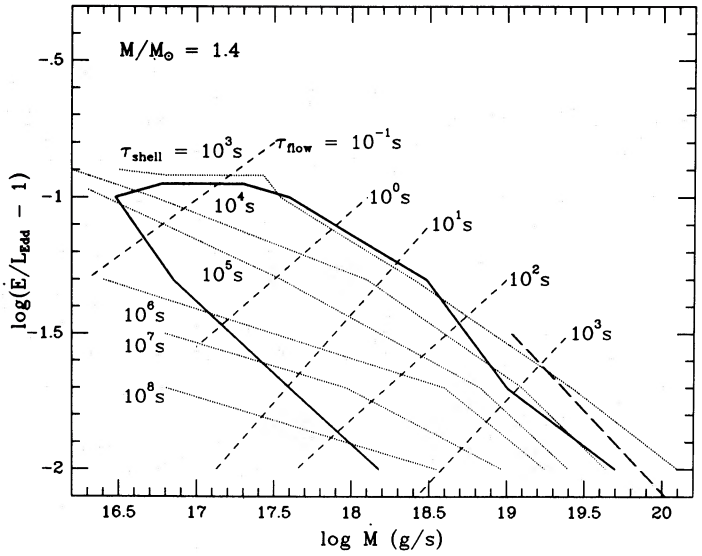

FIG. 2a

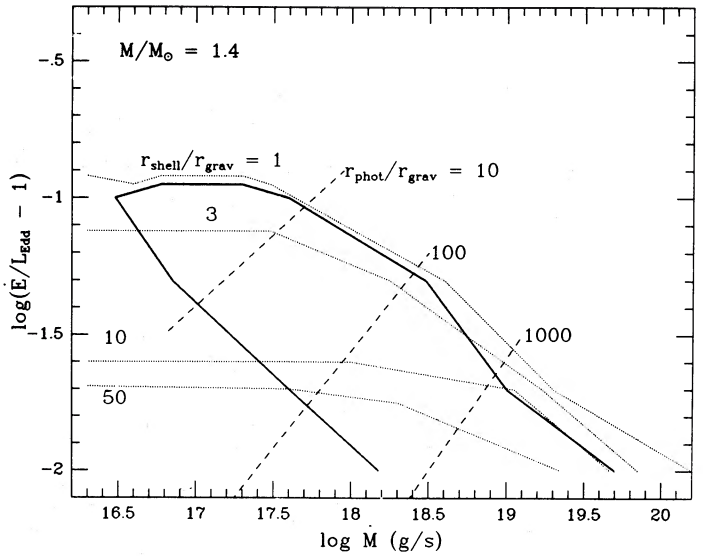

FIG. 2b

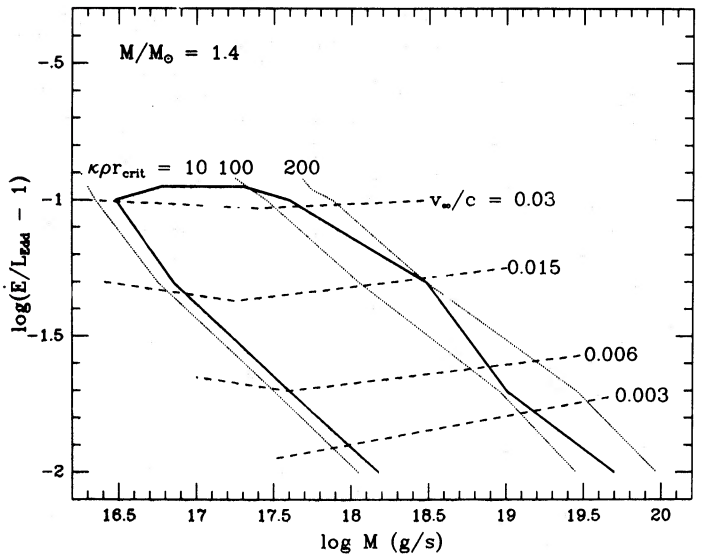

FIG. 2c

FIG. 2.—(*a*) Lines of constant τ_{shell} and τ_{flow} for models in the $\dot{M}-\dot{E}$ plane. The region of acceptable models is enclosed by the heavy solid line. The region where the mass criterion for steady-state flow is not satisfied is to the right of the heavy dashed line. The quantity τ_{shell} is the ratio of the mass between the critical point and the nuclear-burning shell to the mass outflow rate $\dot{M}$. The quantity τ_{flow} is the ratio of the mass between the critical point and the photosphere to the mass outflow rate $\dot{M}$. The right-hand side of our acceptable region is determined by $\tau_{shell} > 10\tau_{flow}$. This implies that there must be over 10 times more mass below the critical point that above it. (*b*) Variation of the radius of the photosphere and the inner radius of the nuclear-burning shell in units of the gravitational radius are shown for our models in the $\dot{M}-\dot{E}$ plane. The top of our acceptable region is determined by r_{shell} approaching the gravitational radius. (*c*) Variation of $\kappa\rho r_{critical}$ and v_∞/c for our models in the $\dot{E}-\dot{M}$ plane. The left-hand side of our acceptable region is set by $\kappa\rho r_{critical} \lesssim 10$.

point and the base at which mass and energy are injected (see discussion). All models calculated by Żytkow (1972, 1973) had a total energy flux below the Eddington limit, so they were all beyond the boundary of Figure 1, somewhere to the right and down.

Notice that all our models are above the Eddington limit, but not by much. It may seem that if the luminous flux flowing from below is strongly super-Eddington, then the solutions with a forced outflow should exist also above the limit of 1.11 L_{Edd} that we found with our models. However, above that limit our models were not self-consistent because they failed to reach a state appropriate for nuclear burning above the gravitational radius. If a neutron star has a higher energy-loss rate, the mass outflow must be nonstationary.

We checked our models for self-consistency in many ways. We computed the amount of matter between the critical point and the photosphere and divided this by the mass-loss rate. A characteristic time thus obtained we call τ_{flow}. The lines of constant τ_{flow} are plotted in the $\dot{M}-\dot{E}$ plane in Figure 2*a*. We also calculated the amount of mass below the critical point but above the nuclear burning shell. This, divided by the mass-loss rate, we call τ_{shell}. The lines of constant τ_{shell} are also shown in Figure 2*a*. A steady-state outflow is not possible unless $\tau_{flow} \ll \tau_{shell}$. The thick dashed line in Figure 2*a* corresponds to $\tau_{flow} = \tau_{shell}$. Acceptable models are to the left of that line.

Our models are unacceptable when either the photospheric radius r_{phot} or the radius of the nuclear burning shell r_{shell} becomes comparable to the gravitational radius $r_{grav} \equiv 2GM/c^2$ because of our use of Newtonian gravity. This condition restricts the domain of acceptable models at large energy-loss rates and large mass-loss rates, as Figure 2*b* shows. The inclusion of general relativity, although causing no fundamental difficulty, may modify this boundary of acceptable models in the $\dot{M}-\dot{E}$ plane.

Our crude treatment of radiation transfer in the atmosphere of the wind models becomes unacceptable when the optical depth at the critical point is not large. The lines of constant optical depth parameter $\tau^* \equiv \kappa\rho r_{crit}$ at the critical point are shown in Figure 2*c*. We considered the models with $\tau^* < 10$ unacceptable. This defines the low mass-loss rate boundary of the region of reasonable models in the $\dot{M}-\dot{E}$ plane.

Our treatment of optically thin regions required the outflow velocity to be much smaller than the speed of light (see eq. [14] and the following comments). The lines of constant ratio v_∞/c are shown in Figure 2*c*. This ratio is small for all acceptable models. However, at high energy-loss rates, where general relativity has to be taken into account, $v_\infty/c = 0.03$. When general relativity is included, it may turn out that v_∞ will be large in the

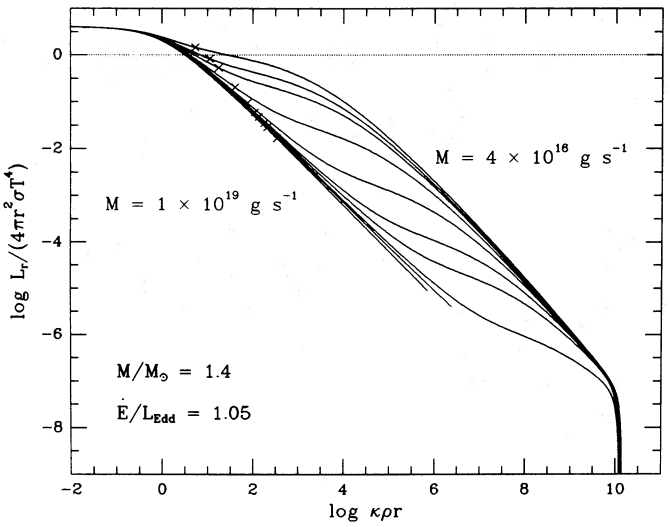

FIG. 3

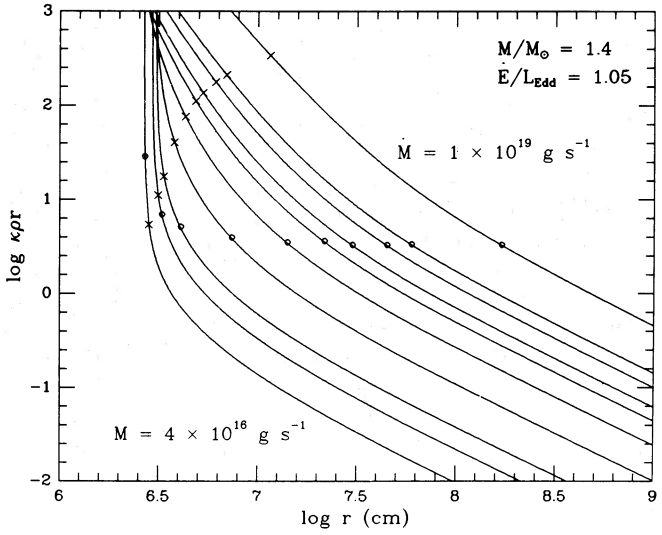

FIG. 4

FIG. 3.—Variation of log $L_r/4\pi r^2\sigma T^4$ vs. log τ^* for models with energy outflow rate $\dot{E} = 1.05\ L_{\rm Edd}$ and the mass outflow of $\dot{M} = 4 \times 10^{16}$, 9×10^{16}, 2×10^{17}, 4×10^{17}, 9×10^{17}, 1.5×10^{18}, 2×10^{18}, 3×10^{18}, 4×10^{18}, and 1×10^{19} g s^{-1}. The location of photospheres is indicated with the dotted line.

FIG. 4.—Variation of the optical depth parameter $\tau^* = \kappa\rho r$ with radius is shown for the same models as in Fig. 3. The crosses and circles represent the critical and photospheric radii, respectively.

models with the highest energy loss-rates. In that case a proper treatment of special relativistic effects may be necessary, which may be difficult.

It is not possible to present all the details for all the models, and there is no reason to do it, since our models are fairly crude. However, we believe it is useful to present details for some of the models, since this may help to develop some feeling for their properties. We will discuss a cross section of the models at a fixed value of $\dot{E} = 1.05\ L_{\rm Edd}$, i.e., the models with log $(\dot{E}/L_{\rm Edd} - 1) = -1.30$ (see Fig. 1), in order to show how "good" models deteriorate at very low and at very high values of mass-loss rate.

Our equations (6) and (7) are designed to provide a proper asymptotic variation of radiation energy density at large radii, where $U_r = L_r/4\pi r^2 c$. This is apparent in Figure 3. In the deep interior we use the diffusion approximation, and $4\pi r^2\sigma T^4 \gg L_r$. We *define* a photosphere of a model by a relation $4\pi r^2\sigma T^4 = L_r$, indicated by the dotted line, just as it is done in a plane-parallel absorbing atmosphere. In all the subsequent figures the location of a photosphere is shown with a small open circle. The location of a critical (i.e., sonic) point will always be indicated with a cross. Also apparent in Figure 3 is how our models switch from being radiation pressure dominated to being gas pressure dominated.

Our treatment of regions with small or moderate optical depth is reasonable, provided the optical depth like parameter $\tau^* \equiv \kappa\rho r$ varies as a power of radius. We find this to be a good approximation at high mass-loss rates, but a poor one at low mass-loss rates, as clearly seen in Figure 4.

The variation of outflow velocity with radius is shown in Figure 5 for 10 models with mass-loss rates between 4×10^{16} and 10^{19} g s^{-1}. It is apparent that v_∞ does not vary much, while the radius at the base of the models (the "shell" radius) varies considerably. This radius is rather large at low mass-loss rates and becomes as small as the gravitational radius at very large mass-loss rates, restricting the domain of acceptable models. The failure of our models at low mass-loss rates is demonstrated in this figure by the photosphere falling below the critical point.

The variation of the temperature with radius in our models is shown in Figure 6. Notice that all the models have very high base temperatures, $\sim 10^9$ K or more, and therefore strongly reduced electron scattering opacity in their interiors.

The variation of density with temperature within the models is shown in Figure 7. All models are radiation pressure dominated near the photosphere, but they split into two families below the critical point. At very large mass-loss rates, the models remain radiation pressure dominated all the way to their bases, and they are almost adiabatic in space, just like Meier's (1982*a*, *b*, *c*) models. This nearly adiabatic behavior

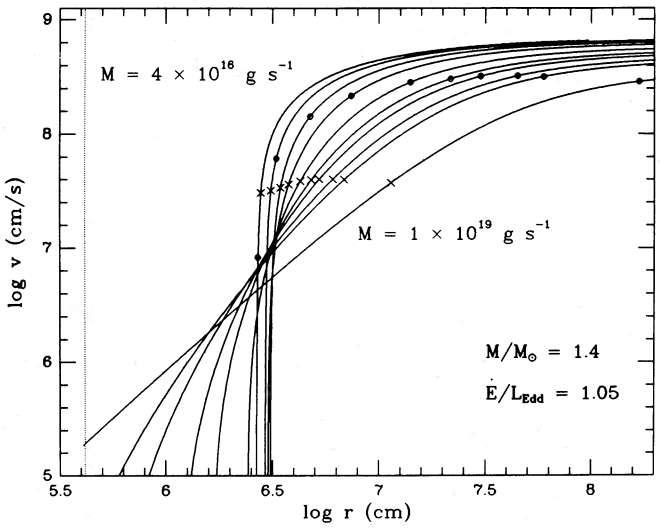

FIG. 5.—Variation of outflow velocity with radius for the same models as in Fig. 3. The symbols are the same. The dotted vertical line marks the gravitational radius.

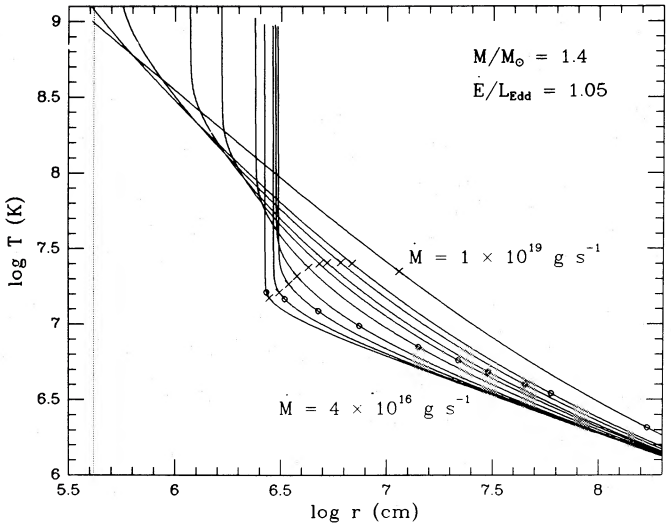

FIG. 6

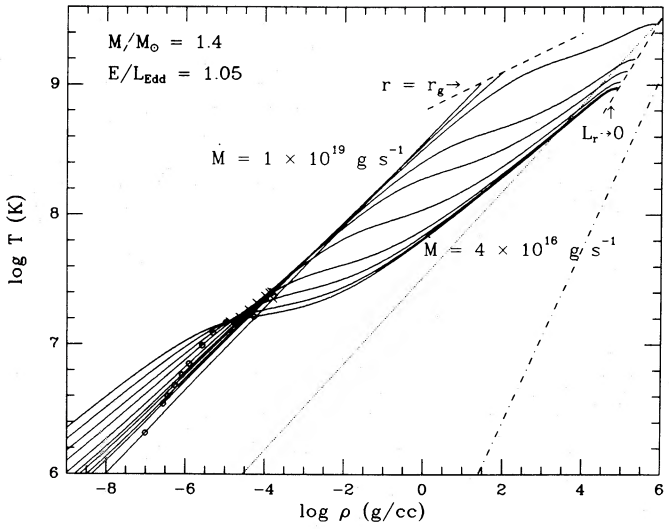

FIG. 7

FIG. 6.—Variation of temperature with radius for the same models as in Fig. 3. The dotted vertical line marks the gravitational radius.

FIG. 7.—Variation of temperature with density for the same models as in Fig. 3. The dashed lines connect the points where the integrations were halted because either the integrated radius became smaller than the gravitational radius, or the bottom of nuclear-burning shell has been reached. Along the dotted line radiation pressure equals gas pressure. Along the dash-dotted line the electron gas becomes degenerate.

makes it impossible to store much mass below the critical point, and the models with the highest mass-loss rates only marginally satisfy the requirement that there should be more mass below the critical point than above it. This requirement is not satisfied by Meier's models. It remains to be seen if the inclusion of general relativity will change this situation. At low mass-loss rates gas pressure becomes important in the deep interiors of the models, and much mass can be stored there. Also, all the low mass-loss rate models can be integrated all the way to the nuclear burning shell, where their luminosity drops to zero. Notice that the high mass-loss rate models were terminated when they reached their gravitational radii, as shown in Figure 7.

All our models had slightly super-Eddington luminosity above their photospheres, and all of them were even more super-Eddington below their critical points. The variation of radiative luminosity with radius is shown for some models in Figure 8. A steep drop of L_r at small radii indicates the location of the helium-burning shell. We should point out that although the luminosity can become highly "super-Eddington" in the interiors as calculated using the Thomson opacity, below the critical point the luminosity always satisfied the relation

$$L_r < \frac{4\pi cGM}{\kappa_e(1+X)}, \qquad (17)$$

where κ_e is given by equation (2).

It is interesting to compare the variation with radius of different energy fluxes: radiative (due to diffusion of radiation), advective (due to bulk outflow of matter), and kinetic (equal to $\dot{M}v^2/2$). The total of these three and the $-\dot{M}GM/r$ term combine to a constant for a given model, the total energy-loss rate $\dot{E}$. The variation of three different energy fluxes with radius is shown for three models: a good one, with a moderate mass-loss rate in Figure 9*a*, a marginal one with a somewhat higher mass-loss rate in Figure 9*b*, and a bad one, with too high a mass-loss rate in Figure 9*c*. Notice that the kinetic energy is never important in the energy balance, which is not surprising for models which are only slightly super-Eddington (see Meier 1982*a*, *b*, *c*). Also notice that while the mass-loss rate increases, the contribution of advected energy flux increases. In the same sequence the importance of general relativity increases. The large advective energy flux, increasing with decreasing radius, makes steady-state outflow models unreasonable. This point will be discussed in the next section.

Finally, Figure 10 shows the variation of many parameters of our models with the rate of mass loss. It is clear that at low mass outflow rates the models become very thin geometrically: the photosphere is very close to the nuclear-burning shell. At large mass outflow rates the radius of the nuclear-burning shell becomes comparable to the gravitational radius, and there is

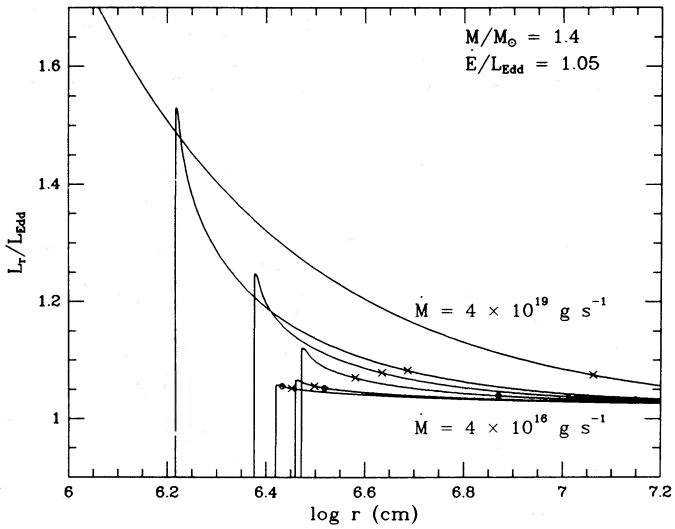

FIG. 8.—Variation of diffusive photon luminosity (in the frame comoving with matter) with radius is shown for models with the mass outflow rates $\dot{M} = 4 \times 10^{16}$, 9×10^{16}, 4×10^{17}, 9×10^{17}, 1.5×10^{18}, and 1×10^{19} g s^{-1}. The crosses mark the critical radii. The open circles mark the photospheres.

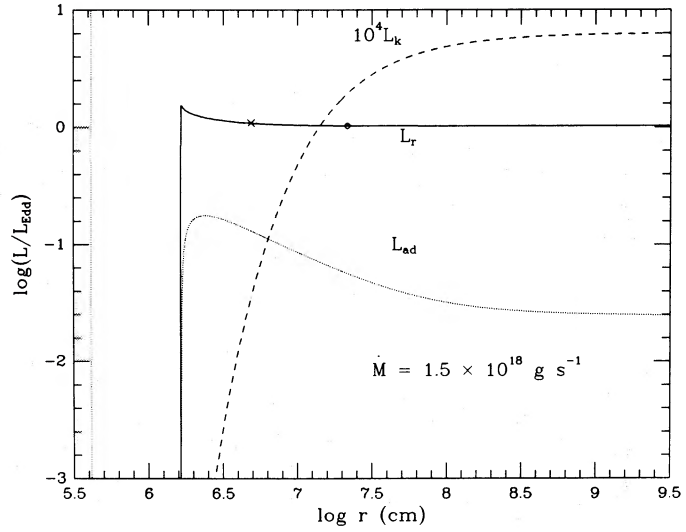

FIG. 9*a*

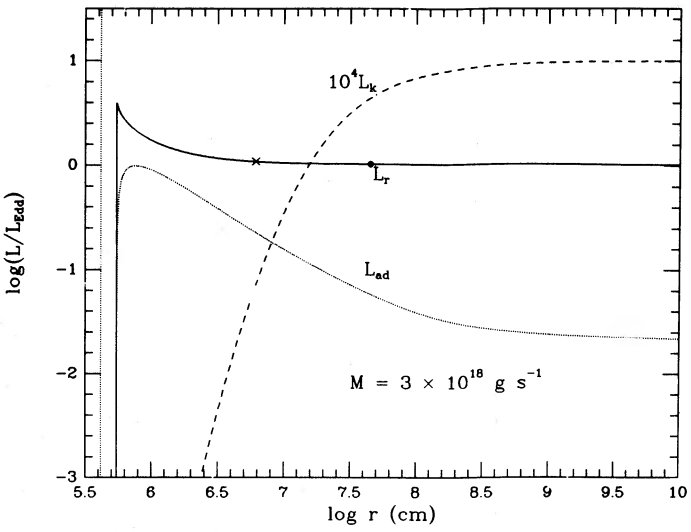

FIG. 9*b*

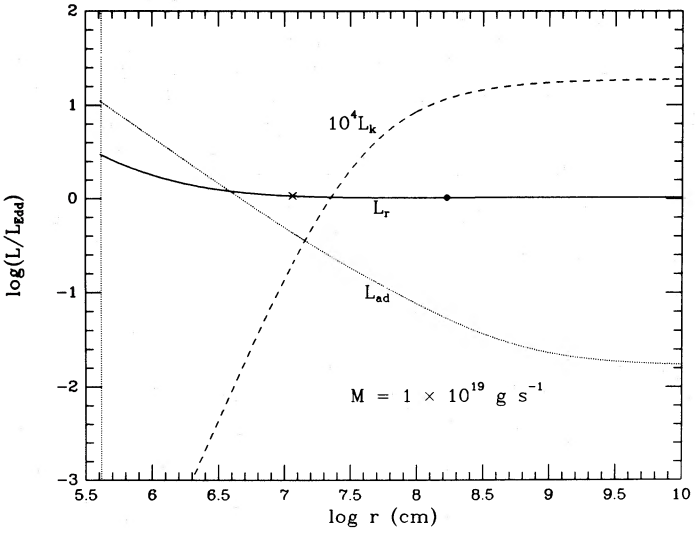

FIG. 9*c*

FIG. 9.—(*a*) Variation of kinetic energy flux ($L_k = \dot{M}v^2/2$), diffusive photon luminosity in the comoving frame (L_r), and advected luminosity ($L_{ad} = \dot{M}[U + P]/\rho$) with radius for an acceptable model with the energy outflow rate $\dot{E} = 1.05\ L_{Edd}$ and the mass outflow rate $\dot{M} = 1.5 \times 10^{18}$ g s^{-1}. Notice that kinetic energy flux is multiplied by a factor 10^4. The stellar mass is 1.4 $M_\odot$. (*b*) Variation of kinetic energy flux, diffusive photon luminosity, and advected luminosity with radius for another acceptable model with $\dot{E} = 1.05\ L_{Edd}$ and $\dot{M} = 3 \times 10^{18}$ g s^{-1}. The stellar mass is 1.4 $M_\odot$. (*c*) Variation of kinetic energy flux, diffusive photon luminosity, and advected luminosity with radius for an unacceptable model with $\dot{E} = 1.05\ L_{Edd}$ and $\dot{M} = 1 \times 10^{19}$ g s^{-1}. The stellar mass is 1.4 $M_\odot$.

too little matter below the critical point compared with the amount of matter between the critical point and the photo sphere, as indicated by the ratio of the two time scales: τ_{shell} and τ_{flow}.

IV. DISCUSSION

In the previous section we presented our results in a large number of figures displaying the variation of many physical quantities within the models. We established the existence of a region in the parameter space, $\dot{M} - \dot{E}$, where our models are self-consistent. That region can be enlarged using more careful treatments as mentioned before. Within the Newtonian approximation our models are limited to only 1.11 of the Eddington luminosity. In all our models the kinetic energy flux of outflowing matter is below 10^{-3} of the Eddington luminosity, and the outflow velocities at infinity are only a small fraction of the speed of light. There is a practical consequence: our integration constant $\dot{E}$ is almost identical with the photon luminosity as seen by a stationary observer at a large distance from the star.

It is convenient to express the mass-loss rates in units related to the Eddington luminosity. Let us define M^* as

$$M^* = L_{Edd}\, c^{-2} = \frac{4\pi GM}{0.2(1 + X)c}\,. \tag{18}$$

For our star of 1.4 $M_\odot$ with no hydrogen we have $M^* = 4 \times 10^{17}$ g s^{-1}. The mass-loss rates we find with our models are between 3×10^{16} and 3×10^{19} g s^{-1}, i.e., within a

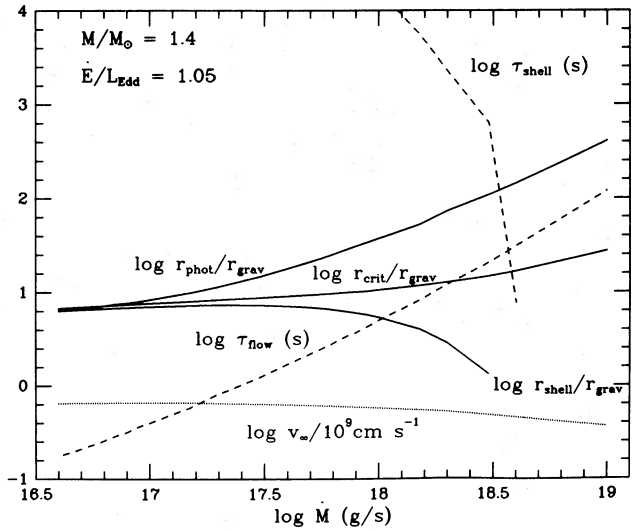

FIG. 10.—Variation of parameters with mass outflow rate $\dot{M}$ at constant energy outflow rate $\dot{E} = 1.05\ L_{Edd}$. The quantity τ_{flow} is the time scale of the flow in the envelope calculated by dividing the mass between the critical point and the photosphere by $\dot{M}$. The quantity τ_{shell} is the time scale for the depletion of the mass below the critical point calculated from the mass below the critical point divided by $\dot{M}$.

few orders of magnitude of M^*. However, since outflow velocities are relatively small, the momentum carried by our winds is usually smaller than the momentum carried with radiation.

Almost all our models have photospheric radii much larger than the radii of neutron stars (see Fig. 2*b*). Therefore, their photospheric temperatures are too low to produce significant X-ray emission above a few keV, except for a few models with the highest luminosity and the lowest mass-loss rates.

We have not specified what should be the radii of the underlying stars for our wind models. We found that the radii at the base of the helium-burning shells covered a large range of values, from slightly larger than the gravitational radius, $r_g \equiv 2GM/c^2$, in the models with the highest luminosity, 1.11 $L_{\rm Edd}$, to very large radii in models with luminosities only slightly in excess of the Eddington limit, as shown in Figure 2*b*. This correlation between the shell radius and the model luminosity follows from the dependence of the electron scattering opacity on the temperature. Models may have a high luminosity, provided the opacity is low in their interior, which requires the shell temperature to be very high, which in turn is possible if the shell is at a very high gravitational potential, i.e., at a very small radius. These are the models for which general relativity is important. Also, these are the models which are most interesting, because their shell radii are comparable to the radii of neutron stars. It is clear from Figure 2*b* that stars much larger than neutron stars cannot give rise to winds driven by significantly super-Eddington luminosity.

The atmospheres of our wind models are all sufficiently cool that the electron scattering opacity there is practically constant, equal to the Thomson limit. Also, outflow velocities are almost constant above the photospheres (see Fig. 5). Therefore, the gas density falls off as r^{-2}, and the optical depth parameter $\tau \equiv \kappa\rho r \approx r^{-1}$. This implies that the atmospheres are very extended and cannot be approximated with plane-parallel models, as previously mentioned. Indeed, we found that within our photospheres, defined with a relation $L_r = 4\pi r^2 \sigma T^4$, the optical depth parameter was large, $3 < \tau^* < 12$ (see Fig. 3). In order to predict the emerging spectra, a much more sophisticated treatment of radiation transfer is required. We may say offhand that our models must have spectra different from blackbodies, because they have very extended, electron scattering atmospheres (see London, Howard, and Taam 1984).

Another difficulty in finding self-consistent models with mass outflow shows up below their critical points. The models with large mass-loss rates have almost adiabatic interiors. This was noticed by Meier (1982*a*, *b*, *c*), and it is apparent in the structure of our models as displayed on the density—temperature plane (see Fig. 7): models with large $\dot{M}$ follow a straight line with a slope: $\partial \log T/\partial \log \rho = \frac{1}{3}$ in the region dominated by radiation pressure. This implies that the envelope mass varies only logarithmically with radius, and it is difficult to store enough matter below the critical point to justify the assumption that mass outflow may be treated as a steady-state phenomenon. The adiabatic nature of these models implies that when the electron scattering opacity decreases in the deep interior, the diffusive luminosity increases, always staying very close to the critical value. The specific entropy stays very high, as indicated by the very large ratio of radiation to gas pressure. It is not possible to generate so high a specific entropy with nuclear burning. Therefore, it is not possible to fit models with high rates of mass loss onto a reasonable stellar interior. The models with moderate rates of mass loss depart abruptly from the adiabatic relation (see Fig. 7), and their structure is easier to match to a deep stellar interior within which conventional nuclear reactions generate energy. Meier's models assume that the deep interior of the wind is either adiabatic or radiation pressure dominated, and are, therefore, not appropriate for matching to a stellar interior. If, as in Meier's models, the flow is powered by mass and energy being injected at some radius, an adiabatic solution is appropriate, and having enough mass in the flow below the critical point is not a concern. Therefore, Meier's models are in the region of the $\dot{M} - \dot{E}$ plane where our type of models are not self-consistent (see Fig. 1).

The existence of a well-defined region on the $\dot{M} - \dot{E}$ plane where models with mass outflow are self-consistent indicates that it should be possible to fit some of them to the models of neutron stars with strong bursts due to helium shell flashes. Let us take as an example a model of a 1.4 $M_\odot$ neutron star with a radius equal to $3r_g$, i.e., ~ 12.5 km. Our models have their shell radii equal to $3r_g$ along a line shown in Figure 2*b*. Any wind model on that line may be geometrically attached to the neutron star. The specific entropy in the shell region varies along the line where $r_{\rm shell} = 3r_g$, being low at the left of Figure 2*b* where the mass-loss rate is low, and high at the right where the mass-loss rate is high. Nuclear burning may generate some value of the specific entropy, and this selects the appropriate model in the $\dot{M} - \dot{E}$ plane.

In this study we do not attempt to fit our wind models to models of X-ray bursters. It is clear from a preceding qualitative discussion that such a fit should be possible for some models, but to make it quantitative it is necessary to include general relativity in the wind as well as in the nuclear-burning region. This fitting should be done in a future study.

There seems to be no hope to fit our wind models to white dwarfs with nuclear burning shells. Figure 2*b* indicates that by the time the shell radii are as large as white dwarf radii, i.e., $\sim 10^3 r_{\rm grav}$, the photospheric radii are likely to be very large, and we are in the domain of the models studied by Żytkow (1972). She found that none of those models could store enough matter below the critical point to give rise to a steady-state outflow. Of course, in all those models the temperature was too small to lower the electron scattering opacity in the deep interior. Decrease of opacity below the critical point is a necessary condition for establishment of a steady-state outflow driven by radiation pressure.

It is a pleasure to acknolwedge many stimulating discussions with Tsvi Piran and Paul Joss. We acknowledge support by the National Science Foundation through grant AST-8317116. One of us (T. Q.) acknowledges the support of the Lucy and Eleanor S. Upton Charitable Foundation through a Francis Robbins Upton Fellowship. We also acknowledge the helpful comments of the referee.

REFERENCES

Buchler, J. R., and Yueh, W. R. 1976, *Ap. J.*, **210**, 440.
Cassinelli, J. P. 1979, *Ann. Rev. Astr. Ap.*, **17**, 275.
Cassinelli, J. P., and Castor, J. I. 1973, *Ap. J.*, **179**, 189.
Ebisuzaki, T., Hanawa, T., and Sugimoto, D. 1983, *Pub. Astr. Soc. Japan*, **35**, 17.
Lewin, W. H. G., Vacca, W. D., and Basinska, E. M. 1984, *Ap. J.*, in press.
London, R. A., Howard, W. M., and Taam, T. E. 1984, *Ap. J.*, in press.
Meier, D. L. 1982*a*, *Ap. J.*, **256**, 681.
———. 1982*b*, *Ap. J.*, **256**, 693.
———. 1982*c*, *Ap. J.*, **256**, 706.
Melia, F., and Joss, P. C. 1983, private communication.
Mihalas, D. 1978, *Stellar Atmospheres* (San Francisco: Freeman).
Fowler, W. A., Caughlan, G. R., and Zimmerman, B. A. 1975, *Ann. Rev. Astr. Ap.*, **13**, 69.
Hanawa, T., and Sugimoto, D. 1982, *Pub. Astr. Soc. Japan*, **34**, 1.
Hummer, D., and Rybicki, G. 1971, *M.N.R.A.S.*, **152**, 1.
Kato, M. 1983, *Pub. Astr. Soc. Japan*, **35**, 33.
Paczyński, B. 1969, *Acta Astr.*, **19**, 1.
———. 1983, *Ap. J.*, **267**, 315.
Taam, R. E. 1982, *Ap. J.*, **258**, 761.
Tawara, Y., *et al.* 1984, *Ap. J.* (*Letters*), **276**, L41.
Wallace, R. K., Woosley, S. E., and Weaver, T. A. 1982, *Ap. J.*, **258**, 696.
Żytkow, A. 1972, *Acta Astr.*, **22**, 103.
———. 1973, *Acta Astr.*, **23**, 121.

BOHDAN PACZYŃSKI and THOMAS QUINN: Princeton University Observatory, Peyton Hall, Princeton, NJ 08544